metals

MDPI

Article

Effects of Gravity and Non-Perpendicularity during Powder-Fed Directed Energy Deposition of Ni-Based Alloy 718 through Two Types of Coaxial Nozzle

Pedro Ramiro-Castro [1,*], Mikel Ortiz [1], Amaia Alberdi [1] and Aitzol Lamikiz [2]

[1] TECNALIA, Basque Research and Technology Alliance (BRTA), Paseo Mikeletegi 7, 20009 Donostia-San Sebastián, Spain; mikel.ortiz@tecnalia.com (M.O.); amaia.alberdi@tecnalia.com(A.A.)

[2] Department of Mechanical Engineering, Faculty of Engineering of Bilbao, University of Basque Country, Alameda de Urquijo s/n, 48013 Bilbao, Spain; aitzol.lamikiz@ehu.eus

* Correspondence: pedro.ramiro@tecnalia.com

Received: 20 March 2020; Accepted: 24 April 2020; Published: 26 April 2020

Abstract: The consequences of gravity and the nozzle inclination angle in the powder-fed Directed Energy Deposition (DED) process were examined in this study. We also sought to define guidelines and manufacturing strategies, depending on the DED system configuration and the nozzle type. To do so, two nozzle types were used: a continuous coaxial nozzle with a slit of 0.5 mm and a four-stream discrete coaxial nozzle. Although the main effects of the configurations and the nozzles are well-known, their effects on the clad characteristics and the deposition strategy are as yet unclear. In this paper, measurements of a single clad and the effects of different deposition strategies on cladding applications and inclined walls are presented, and the consequences for manufacturing processes are discussed. Based on a complete study of a single clad, working vertically, five different tilted deposition strategies were applied: three to a single clad and two to an inclined wall. The results for both the single clad and the inclined wall reflect a pattern of changes to height, width, area, and efficiency, at both small and large nozzle angles and deposition strategies. The inclined wall presents a maximum horizontal displacement that can be reached per layer, without geometrical distortions. The amount of material per layer has to be adapted to this limitation.

Keywords: Directed Energy Deposition; continuous nozzle; discrete nozzle; gravity effect; tilting effect; powder; Alloy 718

1. Introduction

Powder-fed Directed Energy Deposition (DED) technology is an Additive Manufacturing process in which a laser beam generates a melt pool on a metallic substrate onto which powder particles are injected. The added particles are fused and integrated into the melt pool before the whole melt pool solidifies, to form a high-quality metallurgical bond between the substrate and the added material. The design is formed layer by layer, thereby permitting the manufacture of complex geometrical parts.

This technology produces near-net-shape geometries that must be finished by a machining process if higher geometric accuracy and surface finish are required. Currently, the hybridization of additive manufacturing and machining processes combines these processes in a single multitask machine, increasing the productivity and the flexibility of the machining process.

Although the use of powder, as described by Toyserkani et al. [1], presents advantages (a wide range of available materials, the possibility of combining different alloys, high surface quality, and low susceptibility to cracking) over the use of wires, not all of the injected powder particles are

deposited directly on the clad. Powder efficiency that entails both productive and economic consequences is therefore an essential factor to consider in the process. Moreover, as explained by Ramiro et al. [2], any waste powder present in the machine room on shavings, in cutting oil, and on the table and the guide rails of the hybrid machine, will generate particular problems with difficult solutions.

Correct nozzle selection is the main factor in generating the most efficient process, which is dependent upon the application of the DED system and its kinematic configuration. There are four different powder injection techniques depending on the application: (I) off-axis powder injection; (II) continuous coaxial powder injection; (III) discrete coaxial powder injection; and (IV) inside-beam powder injection.

The off-axis powder injection was designed for coating shafts and similar geometries where the deposition strategy is unidirectional, as in the laser cladding of a cylindrical steel substrate with multilayer deposits of high-speed steel described by Ur Rahman et al. [3]. Although high efficiency can be obtained, it is not suitable for other geometries.

The continuous coaxial nozzle provides the highest powder efficiency—up to 90% in the work of Zhong et al. [4] due to its concentrated powder stream within a small diameter. In the simulation by Li and Huang [5], the same nozzle type prevented injected particle rebound and the weaker effect of the inner shielding gas on the powder mass flow. Nevertheless, the use of this type of nozzle is only recommended for vertical configurations, due to the negative gravitational effects of a tilted nozzle on the powder mass flow. When this type of nozzle is tilted, the gravitational effect deflects the powder stream, thereby reducing the powder efficiency, as was explained and simulated by Arrizubieta et al. [6]. Nevertheless, it is not clear if it is possible to use it in an efficient way at low tilting angles instead of using another type of nozzle with less powder efficiency.

When manufacturing, coating, or repairing complex geometric shapes, either the cladding nozzle or the substrate must be tilted. In consequence, most machines that either exclusively use or have the option of using the DED process are machines based on a five-axis configuration, as explained by Cortina et al. [7]. Some examples of the complexity of the shapes are the marine engine crankshaft repaired in situ by Torims et al. [8], the semi-sphere coated by Tabernero et al. [9], and the centrifugal compression impeller repaired by Lei et al. [10].

Depending on the kinematic configuration of the DED system, if tilting the substrate is not an option, then the other option is to tilt the cladding nozzle. In such cases, the use of discrete coaxial nozzles is recommended, as such nozzles will minimize gravitational effects on the powder stream. The design of this nozzle type means that the powder stream is not as concentrated as it is from the continuous coaxial type. As a result, the application of powder particles through the discrete coaxial nozzles is less efficient than through the continuous coaxial nozzles, as Ramiro et al. [11,12] found when comparing both types of nozzles. Additionally, perpendicularity between the nozzle and the substrate cannot always be maintained, and this issue will also detract from the efficiency of the material deposition process.

Finally, Zhu et al. [13] achieved the widest tilt range, using the inside beam powder injection method in a laser-processing robot, which proved the better option for in situ repair of large components with complex shapes, when compared to the commercially available nozzles analyzed by Lamikiz et al. [14]. This nozzle is equipped with a more complex laser system that divides the laser beam in a coaxial ring that converges at the same distance while the powder is injected by an internal vertical powder feed.

Although these two effects (gravitational and the non-perpendicularity) are well recognized in qualitative terms, it is not clear how the tilt of the different nozzle types and substrate inclination can affect material deposition. Both effects are very important when defining the material deposition tool paths, as they will affect the geometry of the clad, which is used to define the overlap between the adjacent clads and the layer height. Additionally, it is important to know how powder efficiency is affected, in order to define the optimum deposition strategies for maximum powder efficiency, which becomes especially significant when manufacturing medium to large-size parts.

The literature on laser-cladding design and geometrical aspects is sparse, and most of it is focused on the limits to inclined walls and strategies using coaxial discrete nozzles, while the study of the continuous coaxial nozzle has to some extent been overlooked. Arregui et al. [15] studied the fabrication of walls by defining two strategies, both of which with high inclinations. However, Möller et al. [16] obtained the best results with a third option, by using a tilting table on which to tilt the substrate in relation to a vertically fixed laser head. Recently, Hao et al. [17] simulated the evolution of height, width, and peak point offset, due to gravity and non-perpendicularity, in the geometry of a single clad, demonstrating the effectiveness of their model.

This study was focused on the quantitative evaluation of the effects of gravity and non-perpendicularity when employing different types of (continuous and discrete) coaxial nozzles for depositing powder particles of Alloy 718 material. To that end, the study of single clads was pursued, to ascertain the process parameters to produce the best clads in terms of quality, efficiency (η_p), aspect ratio, and Mass Deposition Rate (*MDR*). Secondly, the effects of tilting and non-perpendicularity on the characteristics of the single clads were studied and, finally, based on the above results, the strategies were selected for multilayer coating of inclined walls.

2. Materials and Methods

2.1. Materials

A nickel-based alloy (Alloy 718) was used in the experimental tests, as both the filler and the substrate material. The filler material consisted of powder with a granulometry between 45 and 150 μm, from Flame Spray Technologies (FST, Duiven, the Netherland), and the substrate material was in an annealed state. Table 1 presents the chemical composition of the powder and the substrate materials. Alloy 718 presents excellent oxidation and corrosion-resistant properties at high temperatures (up to 980 °C), hence its widespread use in the aeronautical sector.

Table 1. Chemical composition of Alloy 718 powder and substrate (wt.%).

Alloy 718	Ni	Cr	Fe	Nb+Ta	Mo	Ti	Al
Powder	52.8	18.5	18	4.8	3.5	0.75	0.3
Substrate	53.5	18.7	17.7	5	2.9	0.94	0.58

2.2. Machine

All tests were performed on an IBARMIA ZVH45/1600 Add+Process hybrid machine (Figure 1). This multi-process machine (Ibarmia, Azkoitia, Spain) combines DED technology with a 5-axis milling and turning (horizontal and vertical) capability. It is equipped with a Precitec YC52 cladding head (Precitec, Gaggenau, Germany), a Sulzer Metco TWIN-10-C Powder Feeder (Oerlikon Metco, Freienbach, Switzerland), and a Yb-Fiber Rofin FL030 3 kW Laser generator (Coherent Rofin, Santa Clara, CA, USA) with a continuous wavelength of 1.07 μm. A 4-stream coaxial discrete nozzle and a coaxial continuous nozzle with a slit of 0.5 mm, both from Precitec, were used.

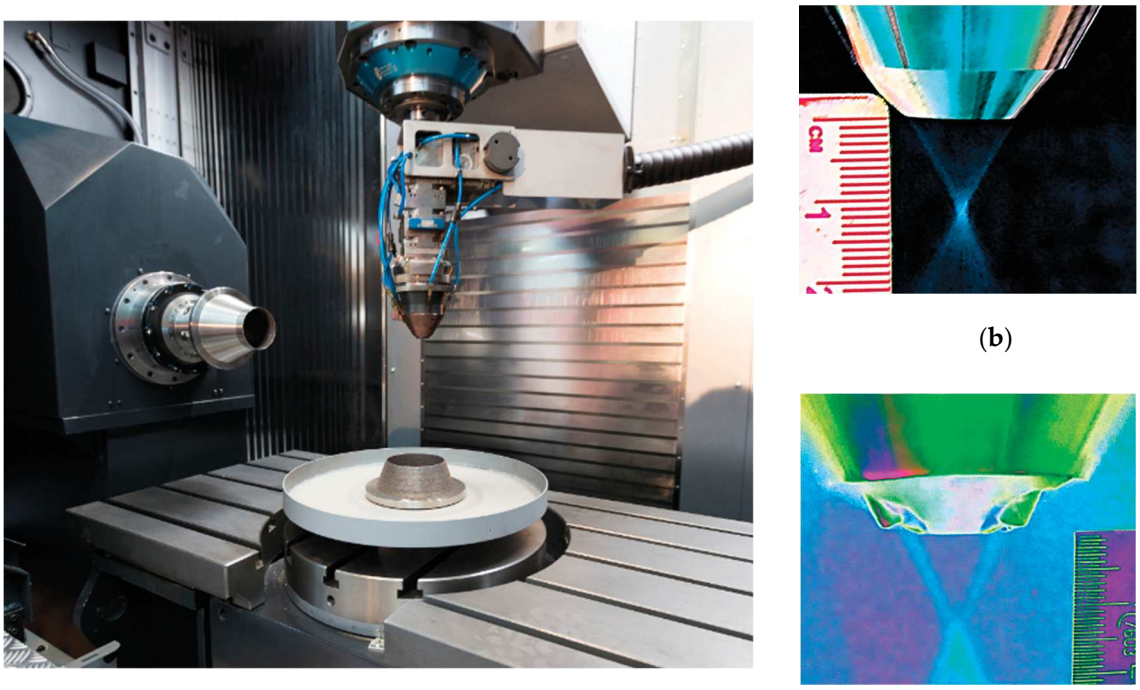

(**a**) (**b**) (**c**)

Figure 1. (**a**) IBARMIA ZVH45/1600 Add+Process hybrid machine; (**b**) continuous coaxial nozzle with a 0.5 mm slit; (**c**) 4-stream discrete coaxial nozzle.

2.3. Experimental Testing

The experimental tests were divided into three different steps. First, single clads were produced under different processing conditions relating to laser Power (P), feed rate (v), and powder mass flow rate ($\dot{m}_p$), with the aim of ascertaining the optimum working conditions for Alloy 718 deposition. Once the best conditions had been established, the gravity-related effects of head tilting and non-perpendicular deposition were analyzed. The results obtained in this analysis were used to define two different strategies for manufacturing inclined walls.

All other processing variables were held constant during the experimentation, considering previous experience. The optimum working distance and laser spot diameter in both nozzles were obtained in the same way as Tabernero et al. [18], as described by Artaza et al. [19]. Their methodology consisted of using containers with different internal diameters for trapping the powder from the powder stream and for measuring the amount of powder collected in each container at different distances from the nozzle [2]. The optimum distance (the distance that collected a higher amount of powder) with that methodology was 11.5 mm for the continuous nozzle and 14.5 mm for the discrete one. Argon was employed as both a carrier and protective gas, at flow rates of 4.5 and 18 $L \cdot min^{-1}$, respectively, using a laser spot size of 2.6 mm. The rotation percentage of the powder feeder defines different powder mass flow rates depending on the fluidity and the density of the powder material. The relation between the powder feeder rotating disk speed percentage and the powder mass flow rate was measured by weighing the powder collected in three minutes.

2.3.1. Single-Clad Testing

Clads of 60 mm in length were manufactured, to explore the optimum processing conditions of Alloy 718, by combining different laser power settings (P), feed rates (v), and powder mass flow rates ($\dot{m}_p$). The settings that were selected for each variable are shown in Table 2. These settings were selected on the basis of the conclusions obtained from previous works. As a result, a total of 72 clads were produced with each coaxial nozzle.

Table 2. Process parameter settings.

Process Parameter	Level
P (W)	1900, 2200, and 2500
v (mm·min^{-1})	300, 500, 700, 900, 1100, and 1300
$\dot{m}_p$ (g·min^{-1})	11, 14, 18, and 21
Type of coaxial nozzle	Continuous (0.5 mm slit), discrete (4-stream)

In the analysis of the cladding, 4 cross-sections were selected at different positions, avoiding the first and the last 10 mm of the clads, thus avoiding process instabilities associated with start and stop conditions, as described by Ocelík et al. [20]. The cross-sections were analyzed in terms of porosity, height (h), width (w), area (A), and dilution depth (b), as shown in Figure 2. Samples were chemically etched by Kalling's N°2 etching and measured with Motic SMZ-143 microscopy (Motic, Hong Kong, China) and Clemex Captiva® software (Clemex, Longueuil, QC, Canada). In addition, the Mass Deposition Rate (MDR), and the powder efficiency (η_p) were calculated by using Equations (1) and (2), where ρ_p is the density of the powder material. The mean value of the 4 sections was applied in models that link the characteristics of the single clad with the main process parameters (laser power, feed rate, and powder mass flow) that were studied. A similar method was followed by Kaiyun et al. [21], working with pre-placed AISI H13 powder, El Cheikh et al. [22] with 316 L powder, and De Oliveira et al. [23] with Nickel–Chromium based alloy powder. The shape of the clad, the process variability of each characteristic, and the error of the empirical models were also analyzed.

$$MDR = A \cdot \rho_p \cdot v \quad (1)$$

$$\eta_p = \frac{MDR}{\dot{m}_p} \quad (2)$$

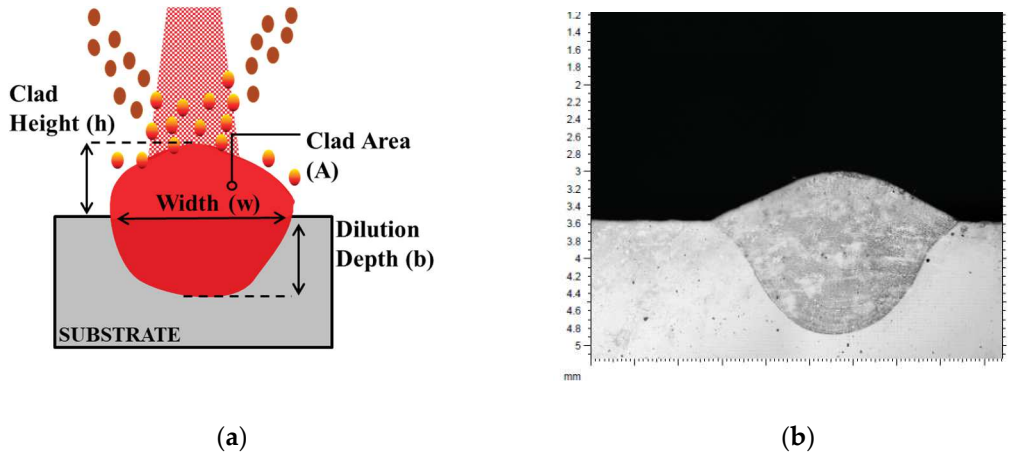

(**a**) (**b**)

Figure 2. (**a**) Characteristics of a single clad; (**b**) macrophotography of a cross-section.

2.3.2. Analysis of the Effects of Head Tilting and Non-Perpendicular Deposition

Testing the single clad helped to define the two optimum deposition conditions for Alloy 718 when employing both the continuous and the discrete coaxial nozzles. The following conditions were considered for the selection: a defect-free cross-section, a Mass Deposition Rate (MDR) higher than 0.5 Kg·h^{-1}, maximum powder efficiency, and an Aspect Ratio (the relationship between clad width and height) between 3 and 5. The latter is related to the appearance of porosity and cracking in overlapping tracks, according to Cárcel et al. [24].

The selected processing conditions were used to perform single tests, using three different strategies to analyze the gravitational effects of head tilting and the effects of non-perpendicular deposition. The angles α and β were defined for that purpose: α represents the tilting angle of the cladding head in relation to the vertical axis, and β represents the inclination angle of the substrate on the horizontal axis. The three strategies can be described as follows:

1. Strategy 1 ($\alpha = \beta$, Figure 3a): the cladding head is tilted and deposition is perpendicular. Thus, in this case, the substrate is inclined, so that perpendicularity is maintained between the head and the substrate, and the head-tilting factor (i.e., gravity) influences the clad characteristics.
2. Strategy 2 ($\alpha = 0$, Figure 3b): the cladding head is held vertical and deposition is performed on an inclined substrate. In this strategy, non-perpendicularity is the factor that influences the clad characteristics, since gravity has no effect on the powder stream.
3. Strategy 3 ($\beta = 0$, Figure 3c): a combination of both effects (tilting and non-perpendicularity). As the combination of Strategy 1 and Strategy 2, it consists of tilting the cladding head on a horizontal substrate. Both the tilting head and non-perpendicularity influence the clad characteristics.

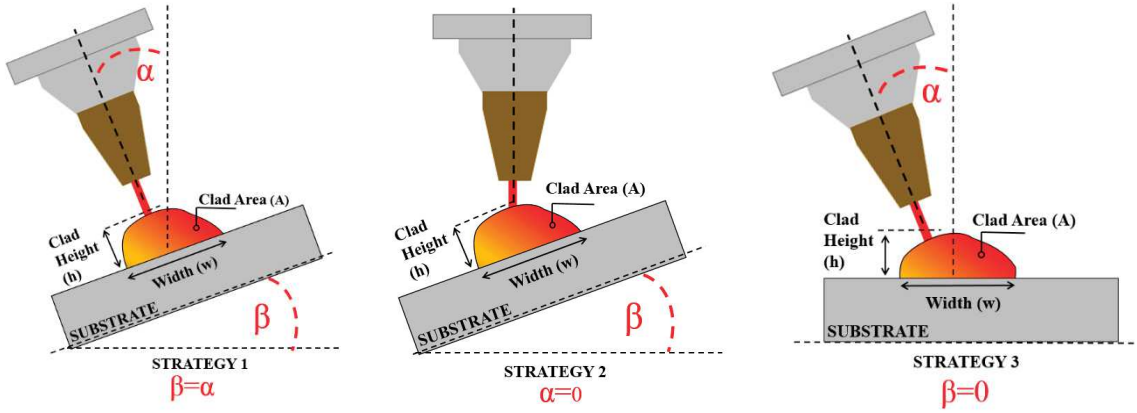

(**a**) (**b**) (**c**)

Figure 3. Strategies for the analysis of the effect of the head tilting and non-perpendicular deposition: (**a**) Strategy 1 ($\alpha = \beta$); (**b**) Strategy 2 ($\alpha = 0$); (**c**) Strategy 3 ($\beta = 0$).

The processing parameters for the study are presented listed in Table 3. As in the previous section, 4 cross-sections of the clads were analyzed, using the same methodology. Finally, the symmetry of the clads was analyzed, using different strategies and different α and β angles. The cross-sections were compared to an empirical model of the cross-sectional area, obtained in Section 2.3.1, as a reference clad to measure symmetry. The model compares the cross-section with a second-degree parabola or a mix of a second-degree parabola and an ellipse, depending on the value of the clad area. The difference between the clad area on both sides of the axis of symmetry of the reference clad was calculated.

Table 3. Process parameters for the analysis of the effect of tilting and non-perpendicular deposition.

Process Parameter	Level
P (W)	2500
v (mm·min^{-1})	500 and 900
$\dot{m}_p$ (g·min^{-1})	14 (Continuous nozzle)-18 (4-stream nozzle)
α or β (°)	0, 5, 10, 15, 20, 25, and 30
Type of coaxial nozzle	Continuous (slit of 0.5 mm), discrete (4-stream)

2.3.3. Manufacturing of Inclined Walls

The objective of this section is to extend the results obtained in the previous sections for a single clad to the generic case of manufacturing inclined walls on a horizontal substrate ($\beta = 0$), which requires multilayer deposits of over one clad per layer. To do so, two strategies were defined (Figure 4):

1. Strategy A (4-axis, Figure 4a): the cladding head is tilted in accordance with the inclination of the wall ($\theta = 90 - \alpha$). Using this strategy, the material is applied in the direction of the wall.
2. Strategy B (3-axis, Figure 4b): the cladding head is maintained in a vertical position ($\alpha = 0$). Using this strategy, the material is vertically applied.

The option of maintaining a perpendicular head and tilting the substrate to manufacture an inclined wall is the easiest option for the multilayer manufacturing of walls with no loss of shape, as was demonstrated by Möller et al. [16]. However, that option requires a tilting table, which was not a feature of the hybrid machine used for this study.

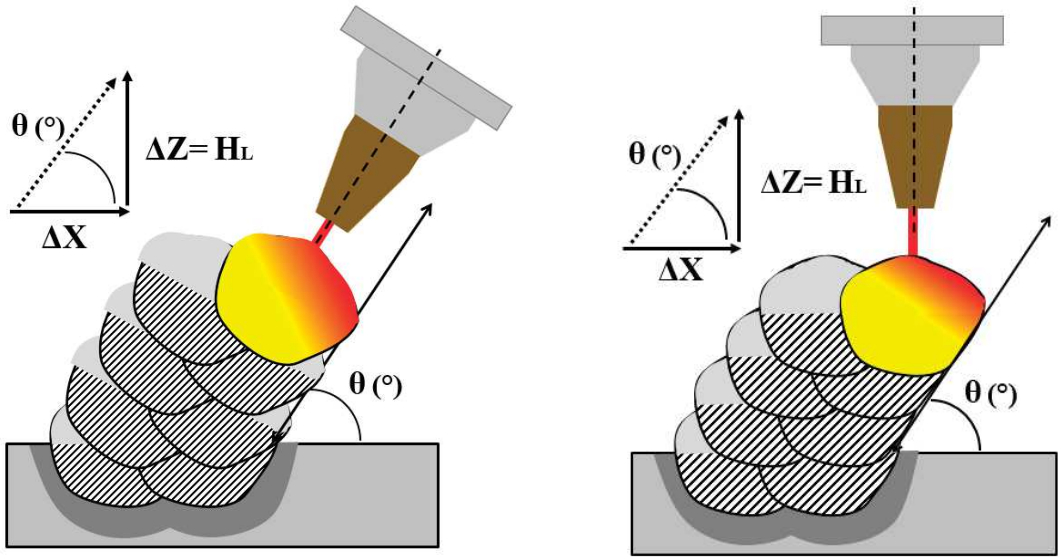

(**a**) (**b**)

Figure 4. Strategies for the manufacturing of inclined walls: (**a**) Strategy A (4-axis); (**b**) Strategy B (3-axis).

The angle of the wall was obtained by defining the horizontal and vertical displacement (ΔX and ΔZ, respectively) in the tool path for each layer. These two displacements were calculated (Equations (3) and (7)) with the desired wall angle (θ), which is related to angle α (from the study of Section 2.3.2) in Strategy A, and the layer height (H_L). The latter was calculated (Equation (4)) by dividing the total area of the layer (A_T) by the sum of the total width (W_T) and horizontal displacement (ΔX), supposing that the material of each layer covers all the area needed to obtain a perfect wall with no waviness (Figure 5a). The total area and the total width of the layer were calculated by using Equations (5) and (6), respectively, where N_C is the number of single clads per layer. The area (A) and the width (w) of the single clad were calculated by using the results obtained in Section 2.3.2 for each specific α and β condition, where d_o is the percentage overlap of the adjacent clads, and K is a correction factor that takes into account the increase of the total width with the number of layers, until a stable width is reached. The phenomenon, shown in Figure 5b, occurs due to the displacement of the melt pool caused by the surface shape of the previous layer and the increased temperature of the wall, and can be reduced by controlling the laser power depending on the temperature measurement, as described by Möller et al. [16]. The number of layers of each wall (N_L) was 30.

The process parameters for the laser-beam multilayer deposits to build the walls are shown in Table 4. The overlap percentage and the dwell time were selected from previous works. To evaluate the effects of inclination on the geometry of the wall, the distance between the center lines of the two overlapped clads was in all cases fixed at the same value as for a vertically manufactured wall.

$$\Delta Z = H_L \quad (3)$$

$$H_L = \frac{A_T}{(W_T + \Delta X)} \tag{4}$$

$$A_T = N_c \cdot A \tag{5}$$

$$W_T = w + w \cdot (N_c - 1) \cdot (1 - d_o) + K \tag{6}$$

$$\Delta X = \frac{\Delta Z}{\tan\theta} = \frac{-W_T \pm \sqrt{W_T^2 + 4 \cdot \left(\frac{N_C \cdot A}{\tan\theta}\right)}}{2} \tag{7}$$

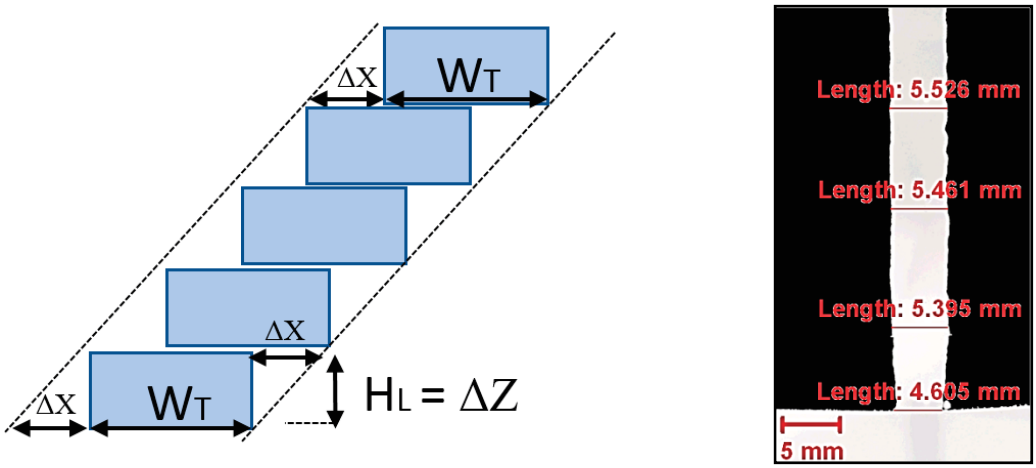

(**a**) (**b**)

Figure 5. (**a**) Scheme of the approach used for calculating the total width; (**b**) increase of the total width with the number of layers.

Table 4. Process parameters for manufacturing inclined walls.

Process parameter	Level
P (W)	2500
v (mm·min^{-1})	500 (900 when it was not possible at 500)
$\dot{m}_p$ (g·min^{-1})	14 (continuous nozzle)-18 (4-stream nozzle)
d_o (%)	50
θ (°)	90, 80, 70, and 60
N_L (-)	30
N_c (-)	2
D_W (s)	5
Type of coaxial nozzle	Continuous (slit of 0.5 mm), discrete (4-stream)

Although the intention was to test both strategies with both types of coaxial nozzles (continuous and discrete), the continuous nozzle was only used in Strategy B, due to the poor results obtained in the analysis of the effects of head tilting and non-perpendicular deposition (Section 2.3.2).

The results were analyzed in terms of geometry, powder efficiency, and *MDR*. In this case, the powder efficiency was calculated by weighing the substrate before and after deposition (m_i and m_f, respectively) and using Equation (8), where t_{DED} is the processing time of the DED process. The MDR was calculated by using Equation (2). Finally, the geometry of the wall was evaluated by the total width (W_W), the wall height (H_W), the initial width of the wall (W_i), which is the width of the wall before the increase of the width K, and the length (L_W) of the wall (Figure 6). These dimensions were measured on a cross-section of the wall, with the Clemex Captiva® software. The measured values were compared to the theoretical values obtained with Equations (9)–(12).

$$\eta_p = \frac{(m_f - m_i)}{(\dot{m}_P \cdot t_{DED})} \quad (8)$$

$$H_W = H_L \cdot N_L \quad (9)$$

$$W_i = W_T - K \quad (10)$$

$$W_w = (W_T + \Delta X) \cdot \sin\theta \quad (11)$$

$$L_W = \frac{H_W}{\sin\theta} \quad (12)$$

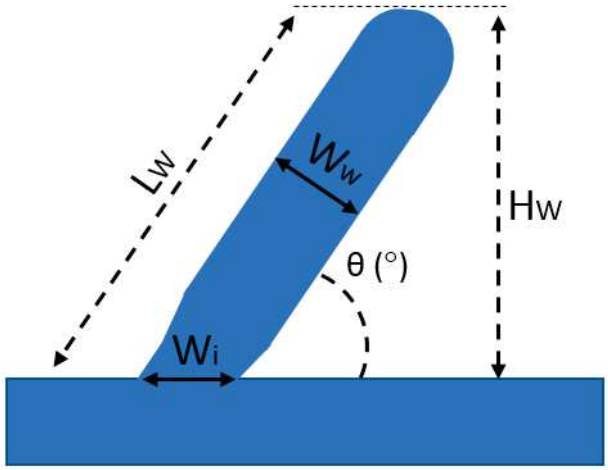

Figure 6. Geometric dimensions of the wall.

3. Results and Discussion

3.1. Single-Clad Testing

Table 5 shows the parameters of the clads that met the requirements presented in Section 2.1 and that were considered suitable for analyzing the effects of gravity and non-perpendicularity.

Table 5. Selected clad parameters and characteristics.

Type of Nozzle	Four-Stream Nozzle		Continuous Nozzle	
$\dot{m}_p$ (g·min^{-1})	18		14	
P (W)	2500		2500	
v (mm·min^{-1})	500	900	500	900
Quality	No defects	No defects	No defects	No defects
Aspect Ratio	3.1	4.84	3.54	4.87
η_p (%)	60.1	51.3	85.4	78.6
MDR (Kg·h^{-1})	0.65	0.54	0.71	0.66

The average values of the four cross-sections of all the clads were used to obtain equations of the single-clad characteristics (width, height, area, and dilution depth), according to the main parameters (laser power, feed rate, and powder mass flow) in the range under study. These equations were obtained by a second-degree polynomial regression and can be used to calculate the parameters needed for manufacturing a single clad with a specific characteristic. Figure 7 shows the evolution of the height and the width at a fixed powder mass flow rate of 14 g·min^{-1} for both nozzles. Similar trends were observed in both nozzles for these two characteristics. Laser power had no significant

effect on the height, although the width increased at higher powers. As expected, both height and width decreased as the feed rate increased.

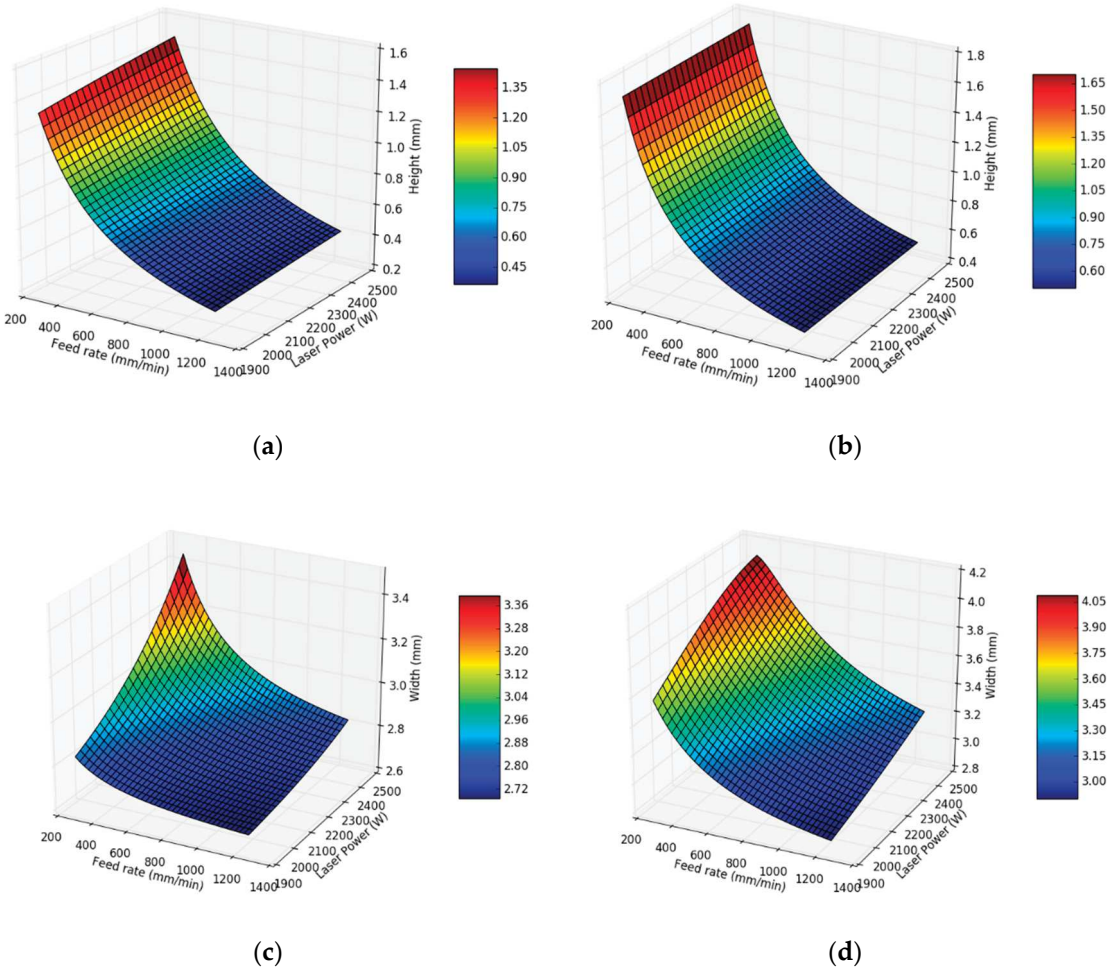

Figure 7. Results of the single-clad study at 14 g·min^{-1}: (**a**,**c**) four-stream nozzle; (**b**,**d**) continuous coaxial nozzle.

The maximum values for powder efficiency and the *MDR* were achieved at a laser power of 2500 W for both nozzles (Figure 8). This is due to the increase of the melt pool size at higher laser power. It must be pointed out that if the energy input becomes excessive the efficiency could be reduced by ablation of the injected powder particles as modeled by Volpp et al. [25]. This possibility has to be considered in recent processes like Extreme High-Speed Laser Material Deposition (EHLA) [26]. In the case of powder efficiency, different behaviors were observed. While the four-stream nozzle showed an optimum powder mass flow rate that optimized powder efficiency and varied with the feed rate, the effect of the powder mass flow rate on powder efficiency was not significant in the case of the continuous nozzle. On the other hand, when increasing the feed rate, both powder efficiency and *MDR* decreased in both nozzles. This is due to the decrease of the size of the melt pool during deposition on the substrate, making the powder catchment lower, as concluded Prasad et al., using a green laser on copper [27]. Finally, the maximum powder efficiency and the maximum *MDR* for the four-stream nozzle and for the continuous nozzle amounted to 64% and 0.75 kg·h^{-1}and 90% and 1.04 kg·h^{-1}, respectively.

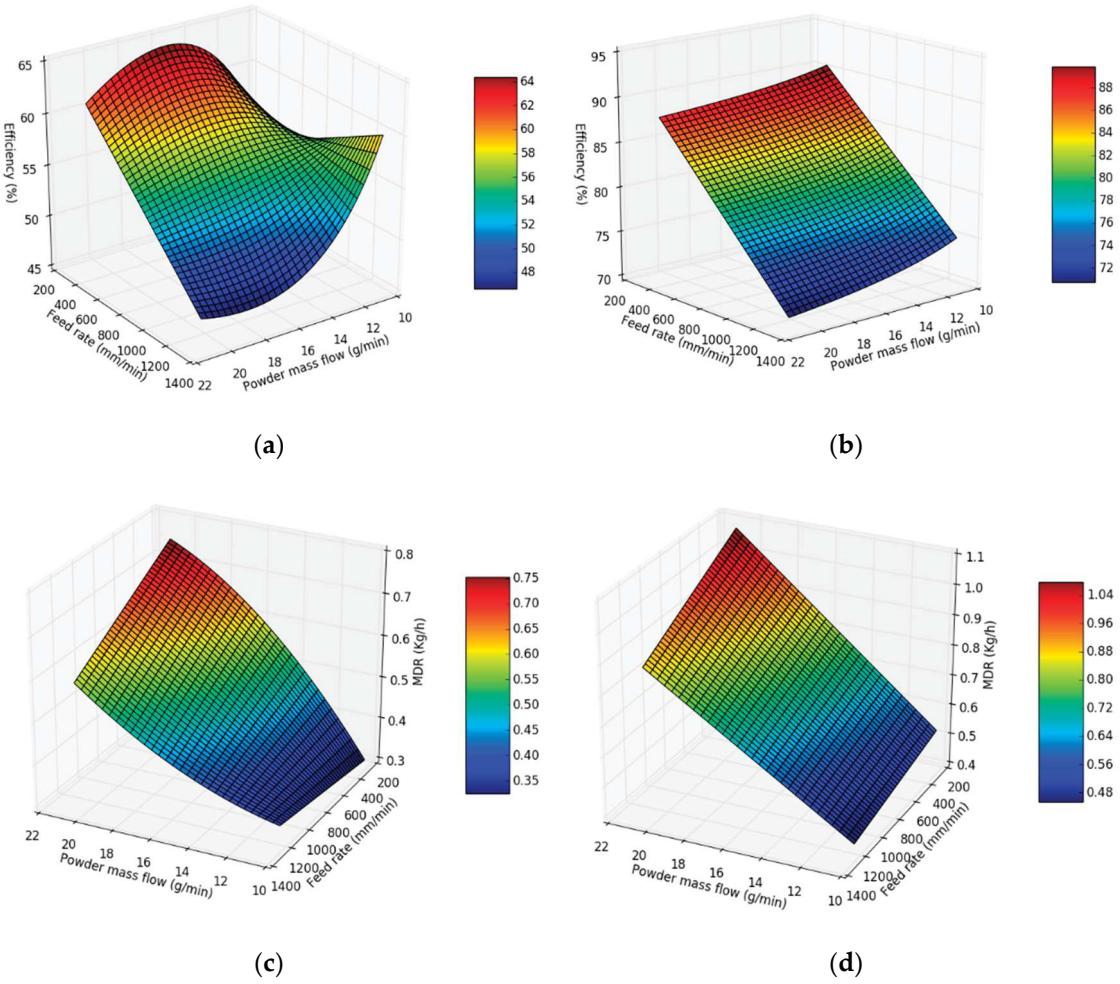

Figure 8. Powder Efficiency and MDR results of the single clad study at 2500 W: (**a**,**c**) four-stream nozzle; (**b**,**d**) continuous coaxial nozzle.

Finally, with regard to the shape of the clad, the average value of the clad area was between the value of a second-degree parabola and an ellipse (Figure 9) and was closer to the second-degree parabola when the area was smaller than 3 mm². With regard to penetration, the average value of the penetration area was also between the value of a second-degree parabola and an ellipse and was closer to a second-degree parabola when smaller than 3.5 mm².

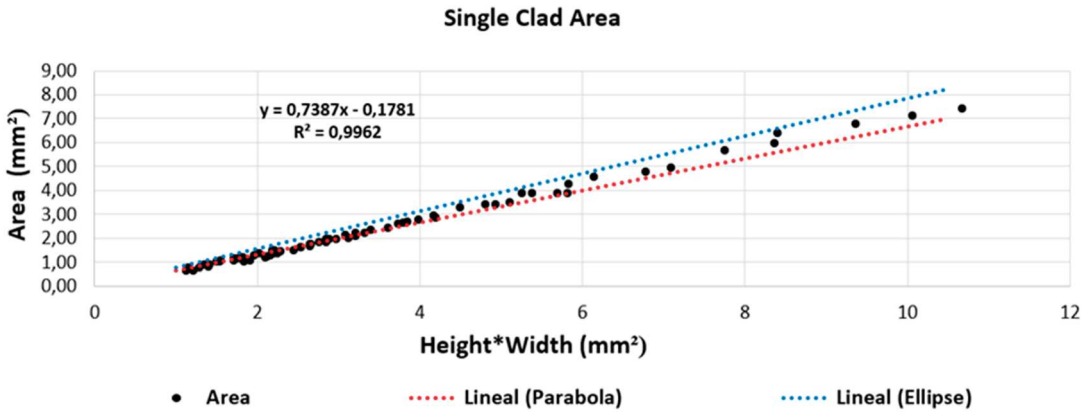

Figure 9. Comparison of the clad areas, using a continuous nozzle with the area of a second-degree parabola (Area = 2·(Height·Width)/3) and an ellipse (Area = Π·(Height·Width)/4).

3.2. Analysis of the Effects of Head Tilting and Non-Perpendicular Deposition

The results of the geometrical dimensions of the clad (h, w, and A) obtained using the different strategies and the different coaxial nozzles at a feed rate of 500 mm·min^{-1} are shown in Figure 10. Those dimensions are presented in comparison with the control clad characterized in Section 3.1 (α = 0, β = 0) at different angles. The graphs of each area are proportional to the *MDR* and the efficiency rate (see Equations (1) and (2)). Similar results were obtained at a feed rate of 900 mm·min^{-1}, as can be seen in Figure 11.

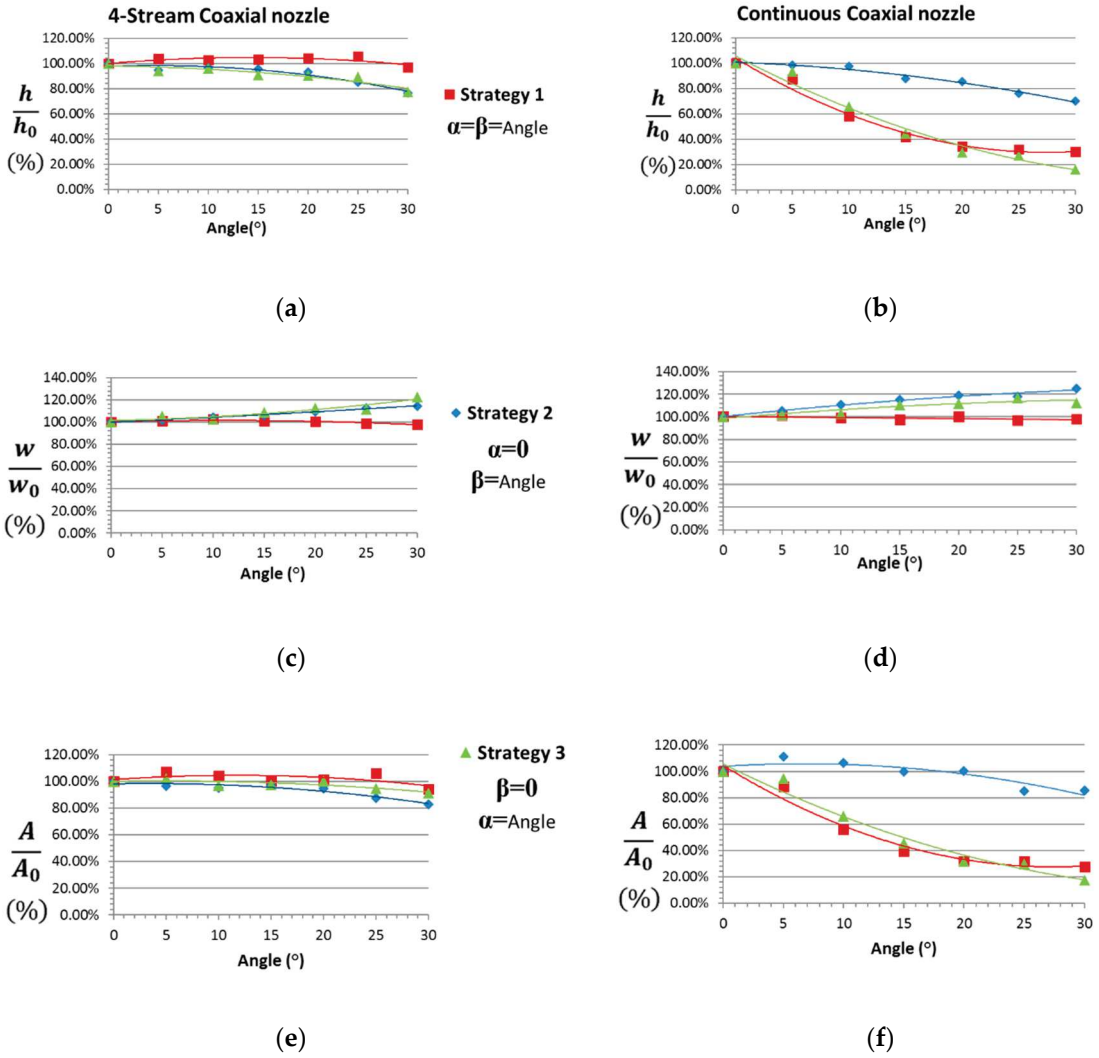

Figure 10. Evolution of the clad dimensions (height, width, and area), in relation to the control clad (α = 0, β = 0), at 500 mm·min^{-1}: (**a**,**c**,**e**) four-stream nozzle; (**b**,**d**,**f**) continuous coaxial nozzle.

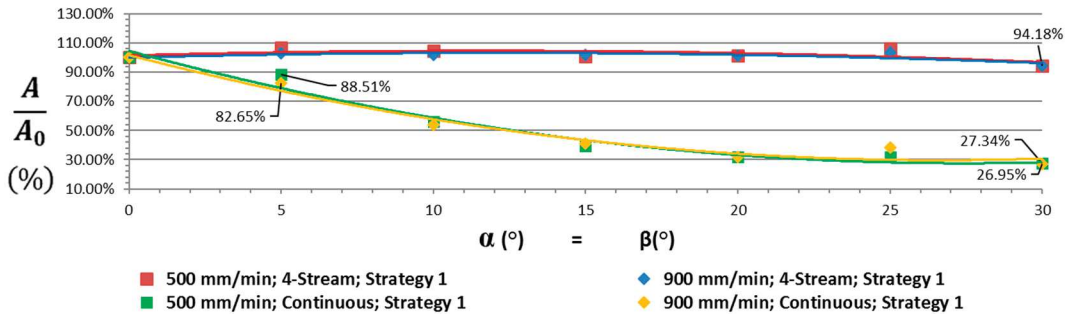

Figure 11. Evolution of the clad area in relation to α and β at 500 and 900 mm·min^{-1}.

As expected, no significant gravitational effects were observed when tilting the four-stream coaxial nozzle (Strategy 1, $\alpha = \beta$). On the contrary, when employing the continuous coaxial nozzle, the clad height was lowered to 87.3% of the height of the control clad at a tilt angle of 5° and to 30.1% at a tilt angle of 30°. Nevertheless, the clad width remained constant at the same feed rate and powder mass flow, as it depends mainly on the spot size and the laser power, which were both constant in this case. As a result, the area was directly proportional to the width and the height (as observed in the Section 3.1), and both the MDR and powder efficiency reflected a very similar proportional relationship with the control clad. The area, the MDR, and powder efficiency were therefore all reduced to 88.5% of the control clad, at a tilt angle of 5°, and to 27.3%, at a tilt angle of 30° (Figure 11). This dimensional reduction, due to the deviation of the powder stream, was caused by gravitational effects. Whereas in the four-stream coaxial nozzle, the powder was injected by four individual pipes with a diameter of 2 mm, forming a powder stream focus, in the continuous coaxial nozzle, the powder was fed into a ring-shaped expansion chamber inside the nozzle, reducing the flow velocity. In this chamber, a homogeneous "powder cloud" was formed which was then fed into a coned-shaped slit of 0.5 mm, leaving the nozzle in the form of a hollow cone. When tilting the continuous coaxial nozzle, the gravity affected the powder homogeneous distribution obtained in the expansion chamber during was fed into the coned-shaped slit, deflecting the powder to the same side (Figure 12). At a higher tilting angle, the deflected amount of powder increased, as did the disturbances in the powder stream caused by the interaction of the powder particles with each other on the same side of the slit. Therefore, it changed the powder stream with the continuous coaxial nozzle functioning more as a lateral nozzle [6] with high divergence, causing a scattered distribution of the powder in the melt pool.

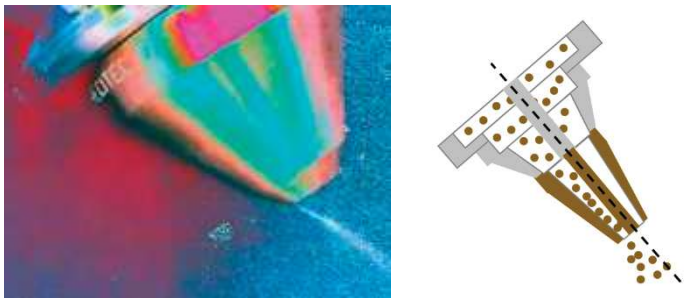

(**a**) (**b**)

Figure 12. Gravitational effect on the continuous nozzle: (**a**) real; (**b**) schematic diagram.

A different behavior was observed when employing Strategy 2 ($\alpha = 0$). In this case, clad height presented a similar trend in both nozzles: a lower height at a larger inclined substrate angle β. It was reduced to 76.7% and to 70% of the control clad, at 30°, with the four-stream nozzle and the continuous nozzle, respectively. In contrast, the clad width as a percentage of the control clad increased as the non-perpendicularity increased, reaching 114.3% and 125.1%, at 30°, for the four-stream nozzle and the continuous nozzle, respectively. This increase occurs due to the elliptical projection of the laser spot on the inclined substrate, which widens the melt pool, and therefore widens the surface on which the powder can be trapped. However, only the continuous coaxial nozzle showed a slight area increases at angles lower than 15° and, consequently, an increase of the efficiency and the MDR. The area, the MDR, and powder efficiency remained constant at angles lower than 20° with the four-stream nozzle. Therefore, a wider melt pool showed a weak effect on the powder catchment that needs to be investigated in further studies. At angles higher than 20°, the area was reduced to 82.8% and 85.8%, at 30°, for the four-stream nozzle and the continuous nozzle, respectively. This reduction occurs because most of the inclined melt pool, where the material was deposited, was off the optimum working distance (where the powder mass flow converges [2,13]). Up until 20°, the reduction in height was related to the surface tension of the melt pool that depended on the balance between several forces, such as the Marangoni force, as explained by Egry et al. [28].

The molten material flow inside the melt pool not only influences its final geometry, but it also affects the reached maximum temperatures, as simulated Arrizubieta et al. in their model of the melt-pool dynamics [29]. In this case, the width widened while the area remained unchanged. Thus, the shape of the melt pool changed to one with less surface area, due to the reduction in height. At angles larger than 20°, the reduction in height was related to the combined effect of surface tension and reduced powder deposition. This change of shape of the melt pool increased the aspect ratio and decreased the wetting angle of the clad (Figure 13). The latter related to the increase of adhesive force to the substrate.

The results obtained when employing Strategy 3 ($\beta = 0$) can be explained by the results obtained with the other two strategies, as it combines the gravitational effect of head tilting (Strategy 1) with the effect of non-perpendicularity (Strategy 2). In the case of Strategy 3, both clad height and clad width were affected by non-perpendicularity when using the four-stream nozzle, and by a combination of both effects when using the continuous nozzle. In the case of the four-stream nozzle, the effects of Strategy 2 and Strategy 3 were similar, although with some differences. Strategy 2 reduced the clad area to 82.8% of the control clad, and Strategy 3 reduced the area to 91.1%. While those results are similar, they point to some differences in the amount of powder deposits that merit further study. In the case of the continuous nozzle, Strategy 3 combined the reduced height of Strategy 1 with the wider width of Strategy 2. As a result, the area that Strategy 3 generated was larger than the area generated by Strategy 1, up until an angle of 20°. At higher angles, the increased width due to non-perpendicularity would be insufficient to compensate for the deviation of the powder mass flow, due to nozzle tilting. Thus, the height and the area of the clads were lower than in Strategy 1. As a result, the area, the MDR, and the powder efficiency varied only slightly when the four-stream nozzle head was tilted, while those same parameters were reduced to 17.5% of the control clad with the continuous nozzle.

Finally, the symmetry of the clad area was observed not to differ from the single-clad study, except for the clads that followed Strategy 1 at 30° (Figure 13). In that case, with a feed rate of 500 mm·min^{-1}, the percentage of the total area separated by the symmetry axis was 42.7% and 57.3%, respectively, where the higher area was deposited in the direction of gravity. In that case, the peak point shifting studied by Hao et al. [17] was obvious.

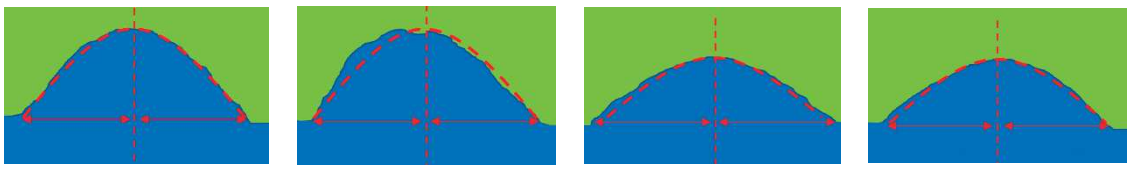

Figure 13. Comparison of the clad shapes (blue color) with the empirical model (red line) when using a four-stream nozzle at different strategies and angles, at $v = 500$ mm·min^{-1}. The aspect ratio increases, and the wetting angle decreased with Strategy 2 and Strategy 3.

3.3. Manufacturing of Inclined Walls

Although walls could be generated at angles between 60° and 90° with the four-stream nozzle and Strategy A (Figure 14), the walls were unsuccessful at angles smaller than 80° when using Strategy B at 500 mm·min^{-1}. Table 6 summarizes the results for powder efficiency and the MDR when manufacturing inclined walls using the different strategies and the different nozzle types.

Table 6. Efficiency and MDR results obtained with different nozzles, strategies, and wall angles (note that the walls that failed are marked with an "X" and walls obtained at 900 mm·min^{-1} are marked with *).

θ (°)	Characteristics	Four-Stream Nozzle		Continuous Nozzle
		Strategy A	Strategy B	Strategy B
90	η_p (%)	54.65	54.10	79.75
	MDR (kg·h^{-1})	0.59	0.58	0.67
80	η_p (%)	55.62	48.65	80.88
	MDR (kg·h^{-1})	0.60	0.52	0.68
70	η_p (%)	54.89	X 48.9*	X X*
	MDR (kg·h^{-1})	0.59	0.53*	
60	η_p (%)	54.53	X 48.1*	X X*
	MDR (kg·h^{-1})	0.59	0.52*	

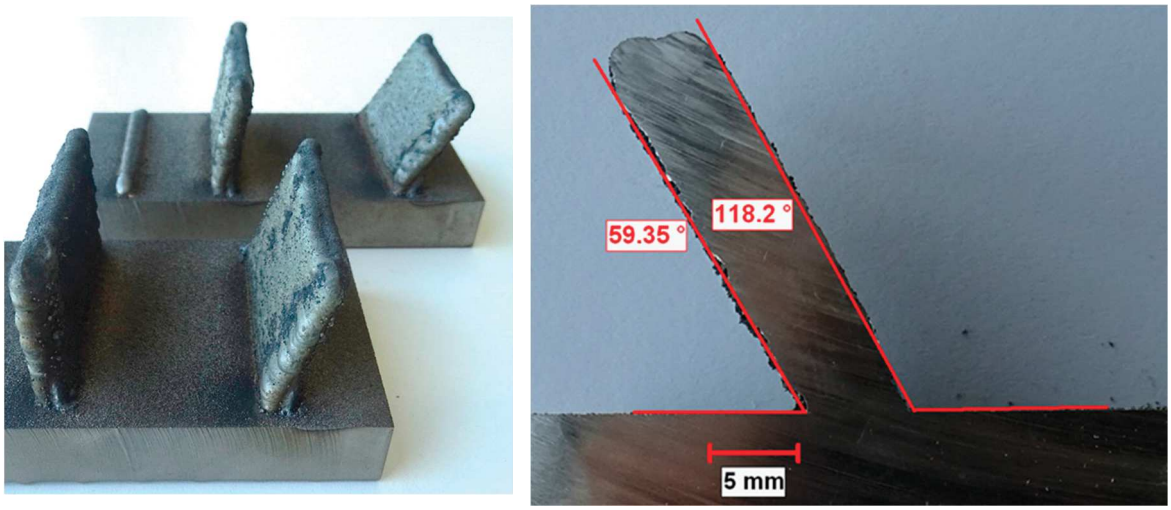

(**a**) (**b**)

Figure 14. Inclined walls manufactured with the four-stream nozzle employing Strategy A: (**a**) wall angles of 60°, 70°, 80°, and 90°; (**b**) cross-section of the wall at an inclination of 60°.

Compared to the single-clad case, at 90°, the efficiency decreased with both nozzles (4–6% less). The maximum powder efficiency and *MDR* values were obtained with the continuous nozzle employing Strategy B, but it was not possible to manufacture walls without defects at angles lower than 80°. Strategy A, with the four-stream nozzle, in all cases generated walls with similar powder efficiency and *MDRs* to the single-clad characteristics resulting from the analysis of the effects of head tilting and non-perpendicular deposition.

The deterioration of the walls with Strategy B at angles smaller than 80° was due to less horizontal clad deposition per layer than the expected ΔX. The material deposited on the edge of the wall has to maintain the shape with low distortion for correct multilayering. The shape of the molten material depends on whether the surface tension and viscosity of the molten material at the DED process temperature are sufficient to withstand the shear stress produced by the gravitational forces. In addition, the time during which gravity can shape the molten material depends on the cooling rate that is, in turn, defined by each strategy.

As with Strategy A, the cladding head was tilted, dilution was directed toward the core of the wall, and the laser beam had an elliptical projection. Thus, the temperature was lower, and dilution into the surface of the wall was shallower. These facts, combined with a wider melt pool and a

decreased clad height, which respectively contributed to a broader surface area securing the clad and to a more stable shape, reduced edge distortion due to gravity, permitting smaller angles. These results with Strategy A and Strategy B differed from the results of Möller et al. [16] that never achieved angles smaller than 70° with the same strategies, using the same parameters as in the vertical-wall case, without considering the evolution of the single-clad characteristics linked to head tilting and the maximum possible value of ΔX.

In contrast, a vertical DED process was employed for Strategy B. The DED process therefore presented no elliptical laser spot projections or changes to the geometry of the molten material. Additionally, as the laser beam was vertical, the temperature and the dilution on the surface of the wall increased, and the shape of the deposited material presented higher distortion due to gravity. This fact reduced the increment on the X axis (ΔX) of each layer, and after several layers, the laser beam was directed toward an area with no additional material. As the minimum value of ΔX at 70° employing Strategy B with both nozzles at 500 mm·min^{-1} was 0.3 mm, it was defined as a new requirement an increment ΔX lower than 0.3 mm with Strategy B. Thus, it was necessary to adapt the process parameters to this requirement. As the walls obtained at 900 mm·min^{-1} could meet this requirement, they were included in the study.

At 900 mm·min^{-1}, it was possible to obtain walls with the four-stream nozzle, but in the walls fabricated with the continuous coaxial one, each new layer presented higher distortion and lack of material in the edges of the wall, reducing the length of the wall progressively (Figure 15). Walls of 20 mm in length were done at the same conditions of the study for showing the severity of this phenomenon in the shape of the wall (Figure 16). Walls at lower laser power (1900 W and employing the equations for the dimensions of single clads) were also done, to reject the melt-pool temperature as a possible cause, but all walls presented the same defect. The good results with the four-stream nozzle with the same strategy suggest the influence of the different powder flow characteristics (trajectory, velocity, powder concentration, etc.) of both nozzles on the melt-pool dynamics as a possible cause. Thus, to obtain walls without distortions with the continuous coaxial nozzle is necessary a $\Delta X < 0.15$ mm per layer, as in the wall obtained at 80°. This requirement sharply reduces the layer height to maintain the wall angle. Further studies with the continuous coaxial nozzle were rejected, because it forces to work at 70° within a range with an efficiency of the single clad similar to the four-stream one, but with an *MDR* lower than 0.5 kg·h^{-1} and, at 60°, out of the range of parameters used in this study, in a range more typical of 1 KW system, like the one used in the works of Bartkowski et al. [30,31].

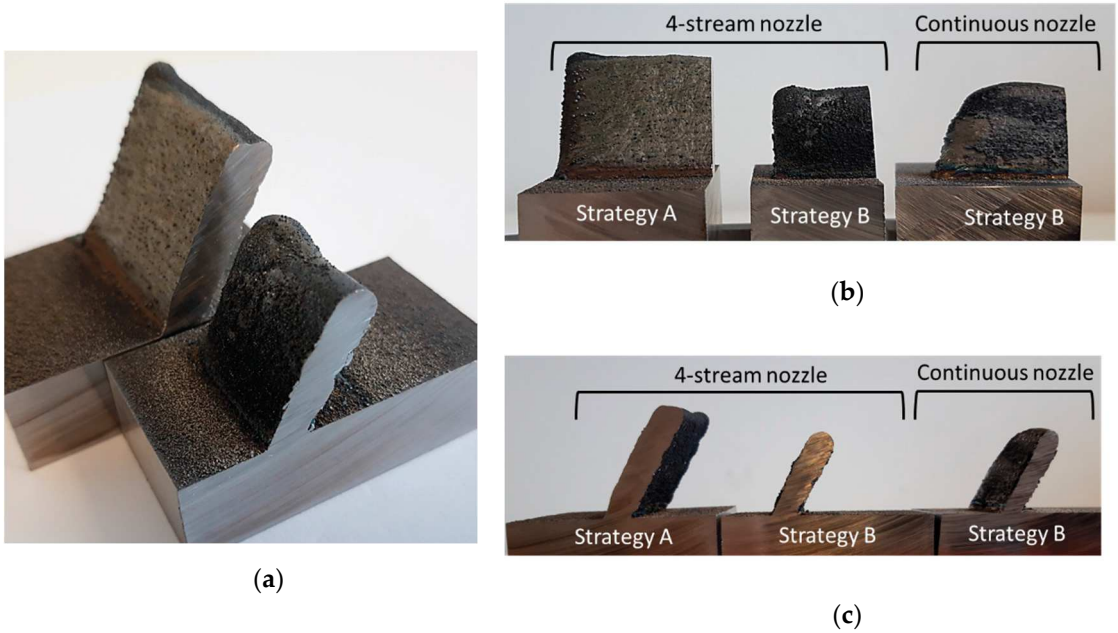

(**a**) (**b**) (**c**)

Figure 15. Walls at 30°: (**a**) comparison of walls fabricated with Strategy A and Strategy B and the four-stream nozzle; (**b**) distortions in the edges of the walls; (**c**) cross-section at different conditions.

The theoretical W_i, L_w, and H_w of the walls at 500 mm·min^{-1} were quite close to the measured values. This fact allows for good approximations of ΔX and ΔZ. On the contrary, the wall width (W_w) presented higher values at smaller angles, compared with the calculated ones, and a high waviness, due to wall edge distortion during the DED process. These effects must be considered in subsequent machining processes, as explained by Ostra et al. [32]. The results with Strategy B at 900 mm·min^{-1} presented the same trend as at 500 mm·min^{-1}. Despite the defects presented by the walls manufactured with the continuous coaxial nozzle, the measured characteristics of the part unaffected by the distortion were quite close to the theorical dimensions, except for W_w, as in the other cases.

(**a**) (**b**) (**c**)

Figure 16. Wall with a length of 20 mm deposited employing continuous coaxial nozzle with Strategy B at 30°. (**a**) wall; (**b**) back view; (**c**) profile view.

When employing Strategy A with the four-stream nozzle, the measured widths and heights presented a pattern in relation to the wall angle: both the measured dimensions of W_i and W_w increased when reducing the wall angle, while the measured values of H_w and L_w decreased, thereby producing wider and shorter walls with the same efficiency. This evolution should be considered when defining the manufacturing toolpaths.

4. Conclusions

The optimum conditions for processing Alloy 718 with DED in terms of quality (no defects) powder efficiency (maximum), *MDR* (>0.5 kg·h^{-1}), and aspect ratio (>3 and <5) were a laser power of

2500 W, a feed rate of 500 mm·min^{-1}, and a powder mass flow of 18 and 14 g·min^{-1} for the four-stream nozzle and the continuous nozzle, respectively. The results obtained for these conditions were a powder efficiency of 60.1% and 85.4%, and an *MDR* of 0.65 and 0.71 kg·h^{-1}, for the four-stream and the continuous nozzle, respectively.

As regards the head tilting effect and non-perpendicular deposition with the four-stream nozzle, the clad characteristics showed no obvious effects of gravity except at 30° with Strategy 1 ($\alpha = \beta$). At that angle, clad asymmetry at 500 mm·min^{-1} in the direction of gravity was higher than in other cases. This is because shear stress resulting of gravity increases with the tilting angle. Before the solidification, at 30° the viscosity is not enough to resist the shear stress. As each layer of the melt pool moves faster than the one just below, the distortion increases with the height. In contrast, Strategy 2 ($\alpha = 0$) and Strategy 3 ($\beta = 0$) presented a widened width and a decreased height and area at a larger angle. Thus, the increases of the width and the reduction of the height reduced distortions of the melt pool caused by shear stress. In addition, the wetting angle decreased increasing the adhesive forces to the substrate.

The gravity effect of the continuous nozzle type strongly reduced the powder efficiency whenever strategies required a tilted head ($\alpha \neq 0$).

As a possible application, tilting the four-stream coaxial nozzle, as per Strategy 3 ($\beta = 0$), could be an interesting option where coatings of lower thickness are required. Contrary to what happens when increasing the feed rate, tilting the nozzle reduces the height, but also increases the width of the clad, with barely any powder efficiency loss. This change of geometry permits a wider range of coating thicknesses, changing only the overlap percentage without changing the DED process parameters.

The strategy and the type of nozzle define the maximum horizontal displacement per layer (ΔX) that can be reached for obtaining inclined walls, without distortions. As the angle of the wall (θ) and ΔX define the layer height and, as a result, the amount of material deposited per layer, it is necessary to select the single clad geometry according to these parameters.

Although Strategy A results in the same powder efficiency and *MDR* for different wall angles, the wall geometry changes, increasing the waviness and generating wider and shorter walls at small wall angles.

In future developments, it would be advisable to address the following aspects:

- To extend the range of angles in this study of the effects of head tilting and non-perpendicular deposition with all the strategies in the case of the four-stream nozzle and only with Strategy 2 in the case of the continuous nozzle.
- To extend the range of angles for the manufacture of inclined walls with both strategies in the case of the four-stream nozzle, without exceeding an ΔX higher than 0.3 mm, employing Strategy B.
- To develop geometric models for coatings and walls by using the Equations for the single-clad characteristics and the evolution of the characteristics linked to head tilting and non-perpendicularity.
- To use the models that are developed to manufacture walls of variable thickness.
- To include the models developed in Computer Aided Manufacturing software, in order to calculate the DED process toolpath, the Computer Assisted Design expected from the DED process, and the subsequent machining toolpath.

Author Contributions: Conceptualization, P.R.-C., M.O., and A.A.; methodology, P.R.-C., A.A., and A.L.; software, P.R.-C.; validation, P.R.-C. and M.O.; formal analysis, P.R.-C.; investigation, P.R.-C.; resources, A.A. and A.L.; data curation, P.R.-C.; writing—original draft preparation, P.R.-C.; writing—review and editing, P.R.-C., M.O., and A.A.; visualization, P.R.-C.; supervision, A.A. and A.L.; project administration, A.A. and A.L.; funding acquisition, A.A. All authors have read and agreed to the published version of the manuscript.

Funding: This research was funded by the European Commission through the project "PARADDISE: a Productive, Affordable and Reliable solution for large scale manufacturing of metallic components by combining laser-based Additive and Subtractive processes with high Efficiency" (Grant Agreement 723440), an initiative of the Public–Private Partnership "Photonics and Factories of the Future". This research was also funded by

European Institute of Innovation & Technology (EIT), through the project "DEDALUS: Directed Energy Deposition machines with integrated process ALgorithms Under dedicated monitoring and control System" (ID 20094), and by the vice-counseling of technology, innovation and competitiveness of the Basque Government (Eusko Jaurlaritza), under the ELKARTEK Program, PROCODA project, grant number KK-2019/00004.

Conflicts of Interest: The authors declare no conflict of interest.

Nomenclature

Symbol	Description	Unit
A	Single clad area	mm^2
A_0	Control clad area	mm^2
A_T	Layer area	mm^2
b	Single clad dilution depth	mm
DED	Directed Energy Deposition	-
d_o	Percentage overlap of adjacent clads	%
D_W	Dwell time between clads	s
h	Single clad height	mm
h_0	Control clad height	mm
H_L	Layer height	mm
H_w	Wall height	mm
K	Wall width correction factor	mm
L_W	Wall length	mm
MDR	Mass Deposition Rate	$Kg\ h^{-1}$
m_f	Weight after deposition	g
m_i	Weight before deposition	g
$\dot{m}_p$	Powder mass flow rate	$g{\cdot}min^{-1}$
N_C	Number of clads per layer	-
N_L	Number of layers per wall	-
P	Laser power	W
t_{DED}	Processing time of the DED process	s
v	Feed rate	$mm{\cdot}min^{-1}$
w	Single clad width	mm
w_0	Control clad width	mm
W_i	Initial wall width	mm
W_T	Total layer width	mm
W_W	Wall width	mm
α	Tilting angle of cladding head on vertical axis	°
β	Inclined angle of substrate on horizontal axis	°
ΔX	Horizontal displacement	mm
ΔZ	Vertical displacement	mm
θ	Wall angle	°
ρ_p	Alloy 718 density	$g{\cdot}mm^{-3}$
σ	Standard deviation	μm

References

1. Toyserkani, E.; Khajepour, A.; Corbin, S.F. *Laser Cladding*, 1st ed., CRC Press: Boca Raton, FL, USA, 2004; pp. 60–61.
2. Ramiro, P.; Ortiz, M.; Alberdi, A; Lamikiz, A. Optimization of the efficiency of the laser metal deposition process applied to high hardness coatings by the analysis of different types of coaxial nozzles. *DYNA* **2018**, *93*, 613–619, doi:10.6036/8836.

3. Ur Rahman, N.; Capuano, L.; Van der Meer, A.; de Rooij, M.B.; Matthews, D.T.A.; Walmag, G.; Sinnaeve, M.; Garcia-Junceda, A.; Castillo, M.; Römer, G.R.B.E. Development and characterization of multilayer laser cladded high speed steels. *Addit. Manuf.* **2018**, *24*, 76–85, doi:10.1016/j.addma.2018.09.009.
4. Zhong, C.; Pirch, N.; Gasser, A.; Poprawe, R.; Schleifenbaum, J.H. The influence of the powder stream on high-deposition-rate laser metal deposition with inconel 718. *Metals* **2017**, *7*, 443, doi:10.3390/met7100443.
5. Li, L.; Huang, Y. Numerical and experimental study on powder stream characteristics in coaxial laser cladding process. In Proceedings of the 6th International Conference on Welding Science and Engineering, Beijing, China, October 2015; Available online: https://www.researchgate.net/publication/282301105_Numerical_and_Experimental_Study_on_Powder_Stream_Characteristics_in_CoaxialLaser_Cladding_Process (accessed on 15 February 2020).
6. Arrizubieta, J.I.; Tabernero, I.; Exequiel Ruiz, J.; Lamikiz, A.; Martínez, S.; Ukar, E. Continuous coaxial nozzle design for LMD based on numerical simulation. *Phys. Procedia* **2014**, *56*, 429–438, doi:10.1016/j.phpro.2014.08.146.
7. Cortina, M.; Arrizubieta, J.I.; Ruiz, J.E.; Ukar, E.; Lamikiz, A. Latest developments in industrial hybrid machine tools that combine additive and subtractive operations. *Materials* **2018**, *11*, 2583, doi:10.3390/ma11122583.
8. Torims, T.; Pikurs, G.; Ratkus, A.; Logins, A.; Vilcans, J.; Sklariks, S. Development of technological equipment to laboratory test in-situ laser cladding for marine engine crankshaft renovation. *Procedia Eng.* **2015**, *100*, 559–568, doi:10.1016/j.proeng.2015.01.405.
9. Tabernero, I.; Calleja, A.; Lamikiz, A.; López de Lacalle, L.N. Optimal parameters for 5-axis laser cladding. *Procedia Eng.* **2013**, *63*, 45–52, doi:10.1016/j.proeng.2013.08.229.
10. Lei, X.; Huajun, C.; Hailong, L.; Yubo Z. Study on laser cladding remanufacturing process with FeCrNiCu alloy powder for thin-wall impeller blade. *Int. J. Adv. Manuf. Technol.* **2017**, *90*, 1383–1392, doi:10.1007/s00170-016-9445-z.
11. Ramiro, P.; Alberdi, A.; Ortiz, M.; Lamikiz, A.; Ukar, E. Characteristics of Fe-, Ni- and Co-based powder coatings fabricated by laser metal deposition without preheating the base material. *Procedia CIRP* **2018**, *68*, 381–386, doi:10.1016/j.procir.2017.12.099.
12. Ramiro, P.; Ortiz, M.; Alberdi, A.; Lamikiz, A. Characteristics of Fe-based powder coatings fabricated by laser metal deposition with annular and four stream nozzles. *Procedia CIRP* **2018**, *74*, 201–205, doi:10.1016/j.procir.2018.08.094.
13. Zhu, G.; Shi, S.; Fu, G; Shi, J; Yang, S.; Meng, W.; Jiang, F. The influence of the substrate-inclined angle on the section size of laser cladding layers based on robot with the inside-beam powder feeding. *Int. J. Adv. Manuf. Technol.* **2017**, *88*, 2163–2168, doi:10.1007/s00170-016-8950-4.
14. Lamikiz, A.; Tabernero, I.; Ukar, E; Martínez, S.; López de Lacalle, L.N. Current designs of coaxial nozzles for laser cladding. *Recent Patents Mech. Eng.* **2011**, *4*, 29–36, doi:10.2174/2212797611104010029.
15. Arregui, L.; Garmendia, I.; Pujana, J.; Soriano, C. Study of the Geometrical Limitations Associated to the Metallic Part Manufacturing by the LMD Process. *Procedia CIRP* **2018**, *68*, 363–368, doi:10.1016/j.procir.2017.12.096.
16. Möller, M.; Baramsky, N.; Ewald, A.; Emmelmann, C.; Schlattmann, J. Evolutionary-based design and control of geometry aims for AMD-manufacturing of Ti-6Al-4V Parts. *Phys. Procedia* **2016**, *83*, 733–742, doi:10.1016/j.phpro.2016.08.075.
17. Hao, J.; Meng, Q.; Li, C.; Li, Z.; Wu, D. Effects of tilt angle between laser nozzle and substrate on bead morphology in multi-axis laser cladding. *J. Manuf. Processes* **2019**, *43*, 311–322, doi:10.1016/j.jmapro.2019.04.025.
18. Tabernero, I.; Lamikiz, A.; Ukar, E.; López de Lacalle, L.N.; Angulo, C.; Urbikain, G. Numerical simulation and experimental validation of powder flux distribution in coaxial laser cladding. *J. Mater. Process. Technol.* **2010**, *210*, 2125–2134, doi:10.1016/j.jmatprotec.2010.07.036.
19. Artaza, T.; Ramiro, P.; Ortiz, M.; Alberdi, A.; Lamikiz, A. Effects of the nozzle tip clogging and the scanning direction on the deposition process during laser metal deposition of alloy 718 using a four-stream discrete nozzle. *Procedia Manuf.* **2019**, *41*, 264–227, doi:10.1016/j.promfg.2019.07.055.
20. Ocelík, V.; Eekma, M.; Hemmati, I.; De Hosson, J.Th.M. Elimination of Start/Stop defects in laser cladding. *Surf. Coat. Technol.* **2012**, *206*, 2403–2409, doi:10.1016/j.surfcoat.2011.10.040.

21. Kaiyun, L.; Xunpeng, Q.; Huaming, L.; Mao, N. Analysis and modeling of melt pool morphology for high power diode laser cladding with a rectangle beam spot. *Opt. Lasers Eng.* **2018**, *110*, 89–99, doi:10.1016/j.optlaseng.2018.05.022.
22. El Cheikh, H.; Courant, B.; Branchu, S.; Hascoët, J.Y; Guillén, R. Analysis and prediction of single laser tracks geometrical characteristics in coaxial laser cladding process. *Opt. Lasers Eng.* **2012**, *50*, 413–422, doi:10.1016/j.optlaseng.2011.10.014.
23. De Oliveira, U.; Ocelík, V.; De Hosson, J.Th.M. Analysis of coaxial laser cladding processing conditions. *Surf. Coat. Technol.* **2005**, *197*, 127–136, doi:10.1016/j.surfcoat.2004.06.029.
24. Cárcel, B.; Serrano, A.; Zambrano, V.; Amigó, V.; Cárcel, A.C. Laser Cladding of TiAl Intermetallic Alloy on Ti6Al4V -Process Optimization and Properties. *Phys. Procedia* **2014**, *56*, 284–293, doi:10.1016/j.phpro.2014.08.173.
25. Volpp, J.; Prasad, H.S.; Kaplan, A. Behavior of heated powder particles on solid surfaces. *Procedia Manuf.* **2018**, *25*, 365–374, doi:10.1016/j.promfg.2018.06.105.
26. Schopphoven, T.; Gasser, A; Backes, G. EHLA: Extreme high-speed laser material deposition. *Laser Tech. J.* **2017**, *14*, 26–29, doi:10.1002/latj.201700020.
27. Prasad, H.S.; Brueckner, F.; Volpp, J.; Kaplan, A. Laser metal deposition of copper on diverse metals using green laser sources. *Int. J. Adv. Manuf. Technol.* **2020**, *107*, 1559–1568, doi:10.1007/s00170-020-05117-z.
28. Egry, I.; Ricci, E.; Novakovic, R.; Ozawa, S. Surface tension of liquid metals and alloys—Recent developments. *Adv. Colloid Interface Sci.* **2010**, *159*, 198–212, doi:10.1016/j.cis.2010.06.009.
29. Arrizubieta, J.I.; Lamikiz, A.; Klocke, F.; Martínez, S.; Arntz, K.; Ukar, E. Evaluation of the relevance of melt pool dynamics in Laser Material Deposition process modeling. *Int. J. Heat Mass Transf.* **2017**, *115*, 80–91, doi:10.1016/j.ijheatmasstransfer.2017.07.011.
30. Bartkowski, D.; Kinal, G. Microstructure and wear resistance of Stellite-6/WC MMC coatings produced by laser cladding using Yb:YAG disk laser. *Int. J. Refract. Met. Hard Mater.* **2016**, *58*, 157–164, doi:10.1016/j.ijrmhm.2016.04.017.
31. Bartkowski, D.; Młynarczak, A.; Piasecki, A.; Dudziak, B.; Gościański, M.; Bartkowska, A. Microstructure, microhardness and corrosion resistance of Stellite-6 coatings reinforced with WC particles using laser cladding. *Opt. Laser Technol.* **2015**, *68*, 191–201, doi:10.1016/j.optlastec.2014.12.005.
32. Ostra, T.; Alonso, U.; Veiga, F.; Ortiz, M.; Ramiro, P.; Alberdi, A. Analysis of the machining process of inconel 718 parts manufactured by laser metal deposition. *Materials* **2019**, *12*, 2159, doi:10.3390/ma12132159.